JOC The Journal of Organic Chemistry

Article

pubs.acs.org/joc

Controlling the Charge Transfer in D−A−D Chromophores Based on Pyrazine Derivatives

Xuefeng Lu,[†] Suhua Fan,[†,‡] Jinhong Wu,[†] Xiaowei Jia,[†] Zhong-Sheng Wang,[†] and Gang Zhou*[,†]

[†]Lab of Advanced Materials & Department of Chemistry, Fudan University, Shanghai 200438, China

[‡]College of Chemistry & Chemical Engineering, Fuyang Normal College, Fuyang, Anhui 236037, China

Supporting Information

ABSTRACT: A series of symmetrical donor−acceptor−donor (D−A−D) chromophores bearing various electron-withdrawing groups, such as quinoxaline (**Qx**), benzo[*g*]quinoxaline (**BQ**), phenazine (**Pz**), benzo[*b*]phenazine (**BP**), thieno[3,4-*b*]pyrazine (**TP**), and thieno[3,4-*b*]quinoxaline (**TQ**), has been designed and synthesized. Intramolecular charge transfer (ICT) interactions can be found for all the chromophores due to the electron-withdrawing properties of the two imine nitrogens in the pyrazine ring and the electron-donating properties of the other two amine nitrogens in the two triphenylamines. Upon the fusion of either benzene or thiophene ring on the pyrazine acceptor unit, the ICT interactions are strengthened, which results in the bathochromically shifted ICT band. Moreover, the thiophene ring is superior to the benzene ring in enlarging the ICT interaction and expanding the absorption spectrum. Typically, when a thiophene ring is fused on the **Qx** unit in **DQxD**, a near-infrared dye is realized in simple chromophore **DTQD**, which displays the maximum absorption wavelength at 716 nm with the threshold over 900 nm. This is probably due to the enhanced charge density on the acceptor moiety and better orbital overlap, as revealed by theoretical calculation. These results suggest that extending the conjugation of a pyrazine acceptor in an orthogonal direction to the D−A−D backbone can dramatically improve the ICT interactions.

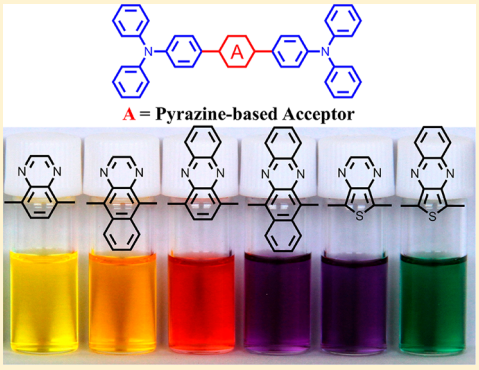

INTRODUCTION

Charge transfer in conjugated organic systems has been widely investigated to construct organic low band gap materials for optoelectronic devices, such as light-emitting diodes (LEDs),[1] photovoltaic devices,[2] field-effect transistors (FETs),[3] nonlinear optics,[4] and fluorescent chemosensors.[5] Such low band gap materials always consist of an electron donor (D) and an electron acceptor (A) connected by a π-conjugated bridge, which facilitates the intramolecular charge transfer (ICT) interactions and therefore lowers the band gap of the organic semiconductor.[6] Among a wide variety of acceptor units, a pyrazine-fused electron-deficient unit has become a quite popular building block[7] to construct conjugated organic materials with low band gap for optoelectronic applications due to its strong electron-withdrawing ability, easy functionalization, and tunable lowest unoccupied molecular orbital (LUMO) levels. For example, pyrazine derivatives, such as quinoxaline,[8] thienopyrazine,[9] pyridopyrazine,[10] fluorinated quinoxaline,[11] pyrazino[2,3-*g*]quinoxaline,[12] thiadiazolo[3,4-*g*]-quinoxaline,[13] and dithienobenzoquinoxaline,[14] have been widely implemented as an electron-deficient comonomers for low band gap polymers which have exhibited promising performance in polymer solar cells (PSCs). Moreover, small organic molecules containing a pyrazine moiety, such as thiadiazolo[3,4-*g*]quinoxaline and pyrazino[2,3-*g*]quinoxaline, have been developed as efficient fluorophores for LEDs[15] and high-mobility semiconductors for FETs,[16] respectively. By proper combination of the donor and pyrazine-based acceptor units, the light-harvesting ability, charge carrier mobility, and condensation structures can be easily tuned. Therefore, it is very necessary to explore a novel pyrazine-based acceptor unit and investigate their structure−property relationship.

Among many conjugated materials with low band gap, the donor−acceptor (D−A) types of chromophores are particularly of interest because their band gap levels and other related properties can be readily tuned through a variety of donors and acceptors. Compared to the conventional D−A chromophores, another donor−acceptor−donor (D−A−D) types of chromophores consist of two electron-donating groups, which will possibly facilitate stronger ICT and therefore further lower the band gap energy.[17] Herein, a series of symmetrical D−A−D chromophores with pyrazine derivatives as electron acceptors have been designed and synthesized (Chart 1). To simplify the comparison system, triphenylamine is used as an electron donor to construct the D−A−D chromophores, and only one pyrazine ring is involved in the central acceptor fragment. Pyrazine derivatives, such as quinoxaline (**Qx**), benzo[*g*]-quinoxaline (**BQ**), phenazine (**Pz**), benzo[*b*]phenazine (**BP**), thieno[3,4-*b*]pyrazine (**TP**), and thieno[3,4-*b*]quinoxaline

Received: April 23, 2014
Published: June 20, 2014

Chart 1. Chemical Structures of the D−A−D Chromophores Based on Pyrazine Derivatives

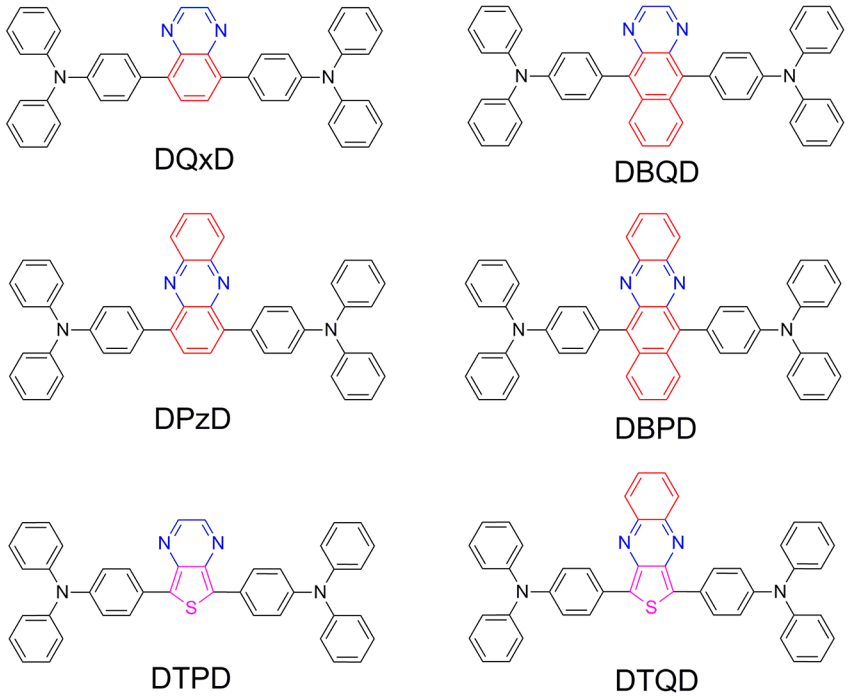

Scheme 1. Synthetic Route for Chromophore DPzD

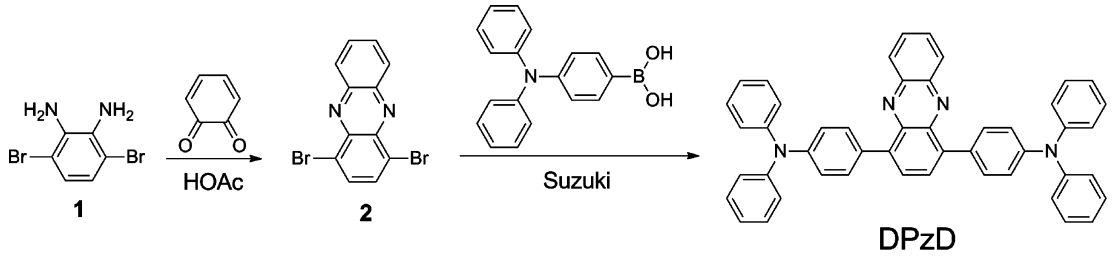

Scheme 2. Synthetic Route for Chromophores DBQD and DBPD

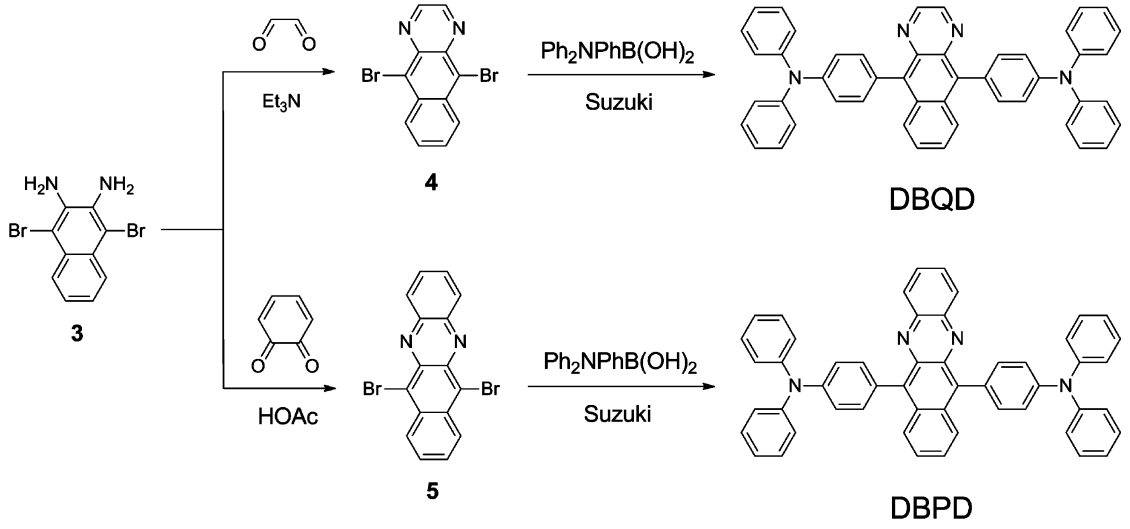

(**TQ**), with different numbers of benzene and thiophene rings are incorporated, respectively. In general, the extension of the conjugation by inserting a benzene or thiophene ring can bathochromically shift the maximum absorption wavelength by less than 50 nm.[18] However, upon the fusion of a benzene or thiophene ring on the pyrazine acceptor, the conjugation extension in the direction vertical to the D−A−D backbone significantly improves the ICT interactions and induces a large bathochromic shift for the absorption maximum. Upon the fusion of a benzene ring on the **Qx** unit in **DQxD**, the

dx.doi.org/10.1021/jo500856k | J. Org. Chem. 2014, 79, 6480−6489

Scheme 3. Synthetic Route for Chromophore DTQD

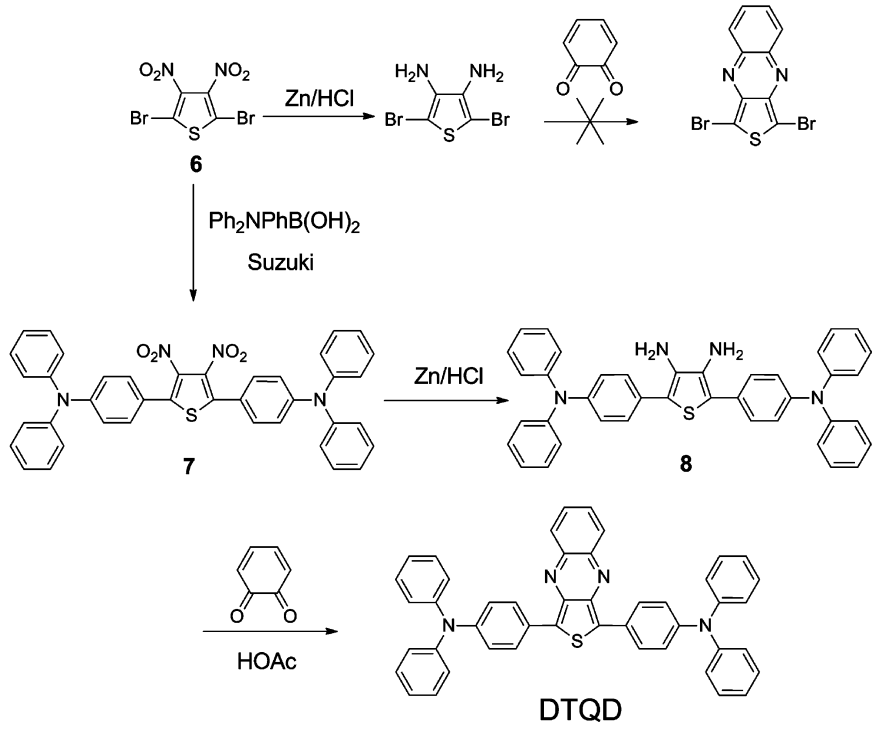

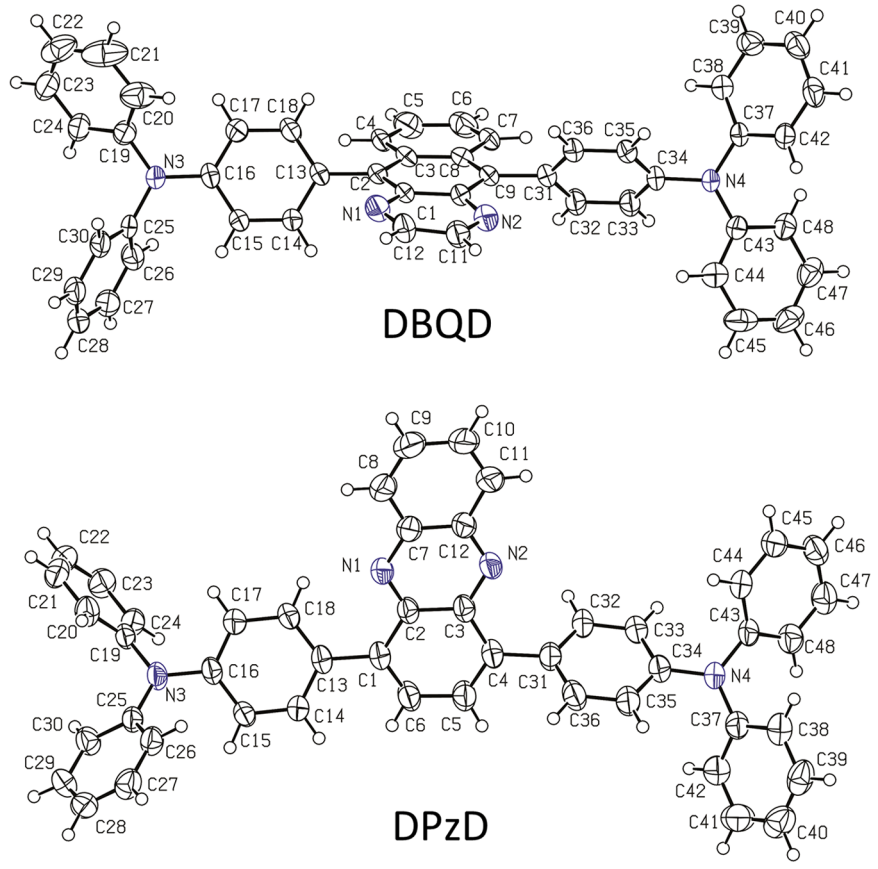

Figure 1. ORTEP diagrams of the molecular structures for isomers **DBQD** and **DPzD**.

maximum absorption wavelength is bathochromically shifted from 413 nm for **DQxD** to 493 nm for **DPzD**, while fusing a thiophene ring on the **Qx** unit further shifts the maximum absorption wavelength to 716 nm by 303 nm for **DTQD**. The theoretical calculation indicates that it stems from the enhanced charge density on the acceptor moiety and better orbital

dx.doi.org/10.1021/jo500856k | J. Org. Chem. 2014, 79, 6480−6489

Table 1. Optic and Electrochemical Properties of the D−A−D Chromophores

	λ_{max}^{Abs} (nm)[a]	ε (M^{-1} cm^{-1})	λ_{max}^{PL} (nm)[a]	Stokes shift (nm)	E_g^{opt} (eV)[b]	E_{HOMO} (eV)[c]	E_{LUMO} (eV)[d]	E_{ox}^{1} (V)[e]	E_{ox}^{2} (V)[e]	ΔE_{ox} (V)
DQxD	413	1.6×10^4	557	144	2.60	−5.06	−2.46	0.26	0.48	0.22
DBQD	455	0.9×10^4	590	135	2.36	−5.05	−2.69	0.25	0.44	0.19
DPzD	493	1.0×10^4	642	149	2.17	−5.04	−2.87	0.24	0.42	0.18
DBPD	560	0.7×10^4	680	120	1.88	−5.02	−3.14	0.22	0.37	0.15
DTPD	544	1.6×10^4	684	140	1.89	−4.92	−3.03	0.12	0.26	0.14
DTQD	716	1.2×10^4			1.43	−4.80	−3.37	0	0.14	0.14

[a]Absorption (λ_{max}^{Abs}) and PL (λ_{max}^{PL}) maxima were measured in DCM solutions (~5×10^{-6} M). [b]E_g^{opt} is optical band gap. [c]The HOMO levels were determined from the first oxidation potentials which were calibrated with ferrocene. [d]$E_{LUMO} = E_g^{opt} + E_{HOMO}$.[17b] [e]The first and the second oxidation potentials.

overlap. Therefore, the controlling of the charge transfer in D−A−D chromophores based on pyrazine derivatives facilitates the understanding of charge transfer in D−A molecules and presents a new way to design D−A copolymers with low band gap for further optoelectronic applications.

RESULTS AND DISCUSSION

Synthesis and Structural Characterization. Chromophores **DQxD** and **DTPD** were synthesized via one-step Suzuki coupling[19] between (4-(diphenylamino)phenyl)boronic acid and 5,8-dibromoquinoxaline and 5,7-dibromothieno[3,4-*b*]-pyrazine,[20] respectively, in high yield. The synthetic approach to chromophore **DPzD** starting from 3,6-dibromobenzene-1,2-diamine[21] is depicted in Scheme 1. Ring closure with cyclohexa-3,5-diene-1,2-dione provided the key intermediate 1,4-dibromophenazine. Then a Suzuki coupling with (4-(diphenylamino)-phenyl)boronic acid produced chromophore **DPzD**. Similarly, chromophores **DBQD** and **DBPD** were synthesized from 1,4-dibromonaphthalene-2,3-diamine.[22] As shown in Scheme 2, ring closure with glyoxal and cyclohexa-3,5-diene-1,2-dione offered intermediate compounds 5,10-dibromobenzo[*g*]-quinoxaline and 6,11-dibromobenzo[*b*]phenazine, respectively, which were then converted to target chromophores **DBQD** and **DBPD** by Suzuki coupling. However, the synthesis of chromophore **DTQD** from the core 1,3-dibromothieno[3,4-*b*]quinoxaline was not applicable due to a poor conversion yield in the ring-closure reaction. An alternative approach was carried out to couple 2,5-dibromo-3,4-dinitrothiophene and (4-(diphenylamino)phenyl)boronic acid first. Then the two nitro groups were reduced to amino groups and converted to a pyrazine ring by condensation with cyclohexa-3,5-diene-1,2-dione to produce chromophore **DTQD** (Scheme 3). It should be noted that the cyclo-condensations of the α-diamines with the α-diones for the target six chromophores were accomplished using two different methods. For chromophores **DQxD**, **DBQD**, and **DTPD**, the condensation with glyoxal was performed with the presence of a weak base, such as triethylamine or sodium carbonate, in ethanol or aqueous solution.[23] While for chromophores **DPzD**, **DBPD**, and **DTQD**, the condensation with *ortho*-quinone obtained by oxidation of catechol with potassium dichromate was carried out in refluxing dichloromethane (DCM) solution using acetic acid as catalyst.[24] The resulting chromophores were characterized by ^{1}H NMR, ^{13}C NMR, and HRMS spectroscopies and were found to be consistent with the proposed structures. In addition, the MALDI-TOF mass spectra (Supporting Information Figure S1) exhibited single intense signals corresponding to the calculated masses of the target chromophores.

To specify the isomeric chromophores **DBQD** and **DPzD**, single-crystal X-ray analysis was performed to provide the most direct description of the molecular structural features. The single crystals of chromophores **DBQD** and **DPzD** were obtained as red, tiny, needle-shaped crystals by diffusion of ethanol into chloroform solutions and slow evaporation at room temperature. Single-crystal X-ray diffraction analysis (Figure 1 and Table S1) indicates that the molecules of chromophore **DBQD** are aligned in a triclinic unit cell with a = 10.685(2) Å, b = 11.672(3) Å, c = 15.495(3) Å, α = 71.759(3)°, β = 83.525(4)°, and γ = 79.610(4)°, while chromophore **DPzD** also exhibited a triclinic structure with cell parameters of a = 9.841(5) Å, b = 10.425(5) Å, c = 19.350(10) Å, α = 78.097(7)°, β = 89.125(7)°, and γ = 73.819(7)°. (Ref: CCDCs 987295 and 987297 contain the supplementary crystallographic data for this paper. These data can be obtained free of charge from The Cambridge Crystallographic Data Centre via www.ccdc.cam.ac.uk/data_request/cif.) It should be noted that the dihedral angle between the central benzene ring in the acceptor moiety and the neighboring benzene ring is distinct for chromophores **DBQD** and **DPzD**. The dihedral angles between the two neighboring phenylene rings in the donor and acceptor parts are found to be 56.4(3)° for chromophore **DBQD** (C3−C2−C13−C18) and 24.4(4)° for chromophore **DPzD** (C2−C1−C13−C18). The more twisted dihedral angle in chromophore **DBQD** is obviously due to the stronger repulsion between the two hydrogens on C4 and C18. Consequently, isomer **DBQD** possesses a more twisted conjugation backbone, which may perturb the effective π-conjugation of the chromophore, accounting for their different optoelectronic properties.

Photophysical Properties. The target chromophores are soluble in common organic solvents, such as DCM, tetrahydrofuran (THF), and toluene. The electronic absorption and the photoluminescence (PL) spectra of the resulted chromophores in DCM solutions were measured at a concentration of ca. 5×10^{-6} M, and the corresponding photophysical data are listed in Table 1. Figure 2 displays the UV−vis absorption spectra of the resulting chromophores in DCM solutions, and it can be found that all the chromophores exhibit two distinct absorption bands. The absorption band in the high-energy region corresponds to the $\pi-\pi^*$ electron transition of the conjugated backbone, and the other one in the low-energy region can be assigned to the charge transfer from the electron-donating triphenylamine unit to the central electron-withdrawing group. As shown in Figure 2, the ICT band of chromophore **DQxD** is located at 413 nm. Upon fusing a phenylene ring on the central quinoxaline unit, the ICT band bathochromically shifts to 455 nm by 42 nm for chromophore **DBQD** due to the extended effective π-conjugation. However, when the phenylene ring is fused on the pyrazine ring instead of the benzene ring of the quinoxaline moiety, a larger bathochromic shift of 80 nm can be observed for chromophore **DPzD** (λ_{max} = 493 nm). This is

dx.doi.org/10.1021/jo500856k | J. Org. Chem. 2014, 79, 6480−6489

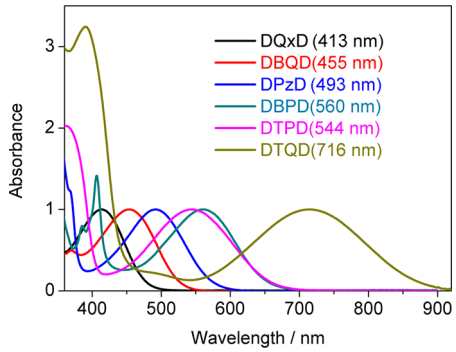

Figure 2. UV−vis absorption spectra of the chromophores in DCM solutions.

obviously due to the less twisted conjugation structure of chromophore **DPzD** as compared to chromophore **DPQD** (Figure 1), which results in a more effective conjugation and stronger ICT interactions. Similarly, the fusion of an auxiliary phenylene ring on the phenazine moiety further bathochromically shifts the ICT band of chromophore **DBPD** to 560 nm. These results suggest that the extension of the conjugation of the pyrazine ring vertical to the direction of D−A−D backbone has a significant effect on the ICT interactions. However, upon replacing **Qx** with **TP**, chromophore **DTPD** exhibits the maximum absorption wavelength at 544 nm with a bathochromic shift of 131 nm in comparison to that for chromophore **DQxD**. This originates from the much stronger electron-withdrawing ability of the **TP** unit as compared to the **Qx** unit.[20b] Interestingly, upon further fusing of a phenylene ring on the **TP** moeity, an organic NIR dye is realized in a simple system. As shown in Figure 2, the absorption spectrum of chromophore **DTQD** covers the whole visible region and extends to the NIR region with the maximum located at 716 nm, which suggested the strongest donor−acceptor ICT interaction in chromophore **DTQD**.

The corresponding PL spectra of the resulting chromophores in DCM solutions were also recorded and are shown in Figure 3. Unlike the absorption spectra, all the PL curves of the D−A−D chromophores demonstrate only one resolved ICT emission band. As shown in Figure 3, chromophore **DQxD** displays the PL maximum at 557 nm. Upon the fusion, an auxiliary phenylene ring, the ICT emission band bathochromically shifts to 590 and 642 nm, respectively, for chromophores **DBQD** and **DPzD** due to the enhanced D−A interactions. The larger

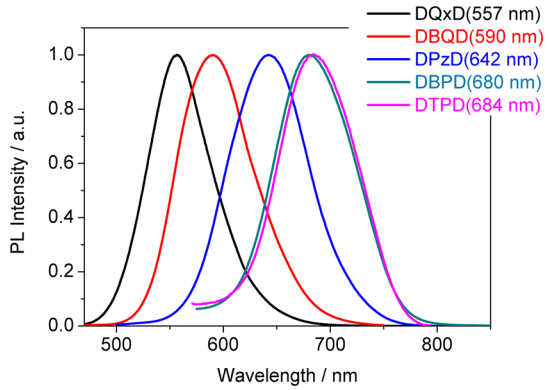

Figure 3. PL spectra of the D−A−D chromophores in DCM solutions.

bathochromic shift for chromophore **DPzD** is due to its more planar structure, which results in stronger ICT interactions similar to the absorption spectra. A further fusion of a phenylene ring on the **Pz** moiety bathochromically shifts the ICT band to 680 nm for chromophore **DBPD**. Moreover, when the fused benzene ring is replaced with thiophene ring, chromophore **DTPD** demonstrates the maximum PL wavelength at 684 nm with a bathochromic shift of 127 nm in comparison to that for chromophore **DQxD**, which is consistent with the trend in their absorption spectra and originates from the much stronger ICT interactions in chromophore **DTPD** as compared to chromophore **DQxD**. However, after further fusing of a phenylene ring on the **TP** moiety, the emission of the NIR chromophore **DTQD** is too weak to be detected in the NIR region by the PL spectrometer. Thus, the trend for the ICT emission maxima is consistent with that for their absorption maxima. For all the chromophores, large Stokes shift over 100 nm (Table 1) can be clearly observed, which is attributed to the ICT nature of the excited state.[25]

Moreover, to further investigate the ICT interactions in the resulting chromophores, the solvatochromic effects on the absorption and PL features for the target chromophores were investigated. The results were quite similar for the tested chromophores because they have close chemical structures. For example, as illustrated in Figure 4, the absorption spectrum of

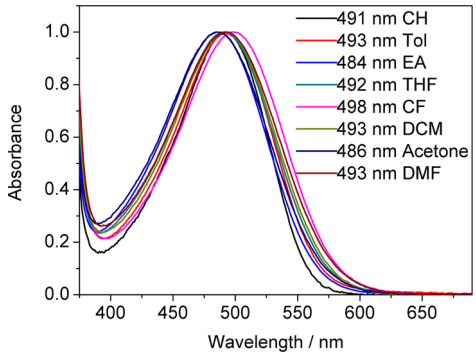

Figure 4. UV−vis absorption spectra of chromophore **DPzD** in different solvents.

compound **DPzD** is slightly solvent-dependent, exhibiting an ICT band ranging from 484 to 498 nm. However, in contrast to the weak solvatochromism in absorption spectra, the differences in the corresponding PL spectra are quite remarkable. Chromophore **DPzD** displays significant solvent-dependent PL (Figure 5), and a bathochromic shift of 74 nm of the PL spectra for **DPzD** can be observed when the solvent polarity increased from cyclohexane (579 nm) to *N*,*N*-dimethylformamide (653 nm). Such a bathochromic shift is characteristic of an efficient charge transfer from the triphenylamine moiety to the central pyrazine-based acceptor. The more significant solvatochromism in PL spectra as compared with that in absorption spectra is probably ascribed to the more polarized excited states.[26] When the electrons are excited from the highest occupied molecular orbital (HOMO) to the lowest unoccupied molecular orbital (LUMO), the dipole is enhanced in the excited S1 state. Therefore, a more polar solvent is able to stabilize such a polarized excited state by the reorientation of the solvent molecules to accommodate the increased dipole,

dx.doi.org/10.1021/jo500856k | J. Org. Chem. 2014, 79, 6480−6489

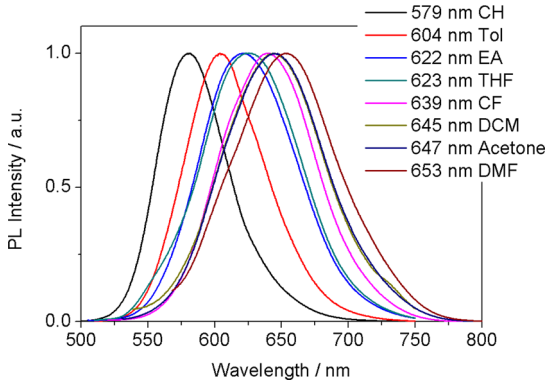

Figure 5. PL spectra of chromophore **DPzD** in different solvents.

lowering the energy of the system and thereby leading to the more distinct bathochromic shift in the PL spectra.[26]

Electrochemical Properties. To further investigate the electronic properties and energy levels of the resulting D−A−D chromophores, the electrochemical behavior was investigated by cyclic voltammetry (CV) (Figure 6) and differential pulse

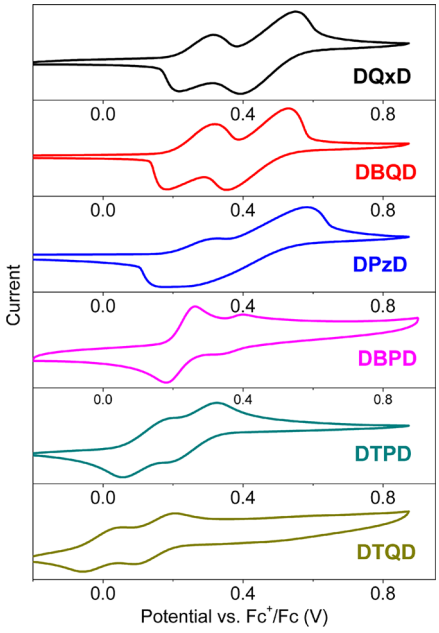

Figure 6. Cyclic voltammograms of the chromophores in DCM solutions.

voltammetry (DPV) (Figure 7), and all data are summarized in Table 1. The CV and DPV measurements were carried out using a typical three-electrode electrochemical cell with a glassy carbon electrode as the working electrode, a Pt electrode as the counter electrode, and a Ag/Ag^+ electrode as the reference electrode in a solution of Bu_4NPF_6 (0.1 M) with a scan rate of 100 mV/s at room temperature under nitrogen.

All the chromophores display two reversible or quasi-reversible redox couples, which correspond to the removal of electrons at the two triphenylamine moieties to form the stable radical cations. As shown in Figure 6, chromophore **DQxD** displays two reversible anodic redox steps at $E^1_{1/2}$ = 0.27 V and $E^2_{1/2}$ = 0.47 V (relative to Fc/Fc^+, the same below), respectively, corresponding to the sequential removal of electrons from the two amine moieties to form **DQxD**$^+$ and **DQxD**$^{2+}$. The two-

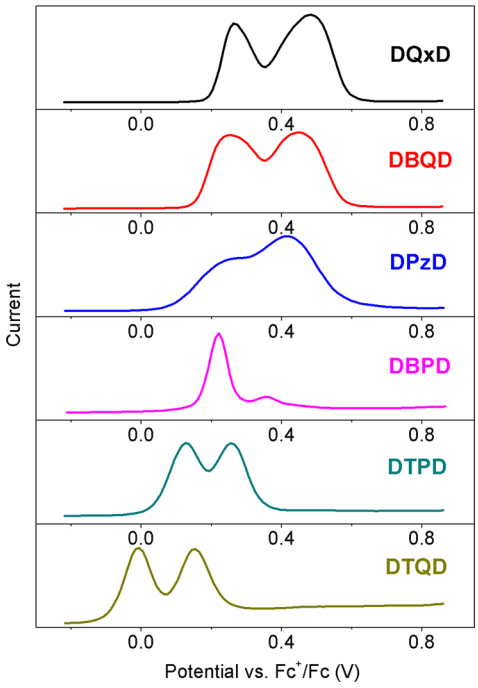

Figure 7. Differential pulse voltammograms of the chromophores in DCM solutions.

step oxidation of the triphenylamine units suggests that the two electrons are successively removed from the two nitrogens in the donor parts and a higher potential is needed to transform the cations into dications. Correspondingly, the DPV of chromophore **DQxD** (Figure 7) also displays two resolved oxidations at 0.26 and 0.48 V. The splitting of the oxidations of two triarylamine units into two steps suggests effective charge delocalization through the D−A−D chromophore in its mixed valence radical monocation **DQxD**$^+$ and effective electron communication between the two arylamine moieties.[27] Upon the fusion of the benzene ring on the central pyrazine derivatives, similarly, chromophore **DBQD** displays two resolved oxidations at 0.25 and 0.44 V, respectively, in both CV and DPV curves, while chromophore **DPzD** exhibits unresolved two-step oxidation at 0.24 and 0.42 V, respectively. With a further fusion of a phenylene ring on the phenazine moiety, chromophore **DBPD** can be oxidized at potential of 0.22 and 0.37 V, respectively. The separation of the oxidation processes implies the electron communication between the two nitrogen centers through the pyrazine-based acceptors.[27] The reason why the second redox peak for chromophore **DBPD** is much weaker is not clear so far. A plausible explanation may be due to the different charge delocalization in **DBPD**$^+$ as compared with other monocations. The relatively close oxidation potentials for the above-mentioned four chromophores are due to the fact that they contain the same electron-donating unit, triphenylamine. However, upon replacing the benzene ring in acceptor **Qx** with a thiophene ring, negatively shifted oxidation potentials for both oxidation processes can be observed for chromophores **DTPD** ($E^1_{1/2}$ = 0.12 V and $E^2_{1/2}$ = 0.26 V). Moreover, the splitting of the two oxidations decreases to ΔE = 0.14 V, indicating a lower electron coupling energy and a weaker electron communication between the two arylamine moieties.[27] The negatively shifted redox potential and the decreased separation of the oxidations for the two arylamine units stems from the different electron-withdrawing ability of

dx.doi.org/10.1021/jo500856k | J. Org. Chem. 2014, 79, 6480−6489

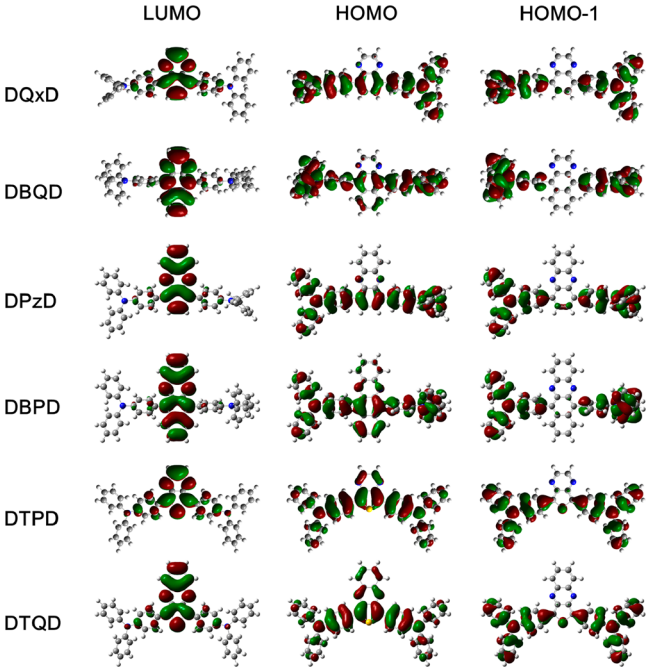

Figure 8. Calculated frontier orbitals of the D−A−D chromophores.

the central pyrazine derivatives which affects the charge delocalization on the chromophores through a contributing inductive effect.[28] This is further proved by replacing the benzene ring in acceptor **Pz** with a thiophene ring. In both CV and DPV curves, chromophore **DTQD** exhibits more negatively shifted two oxidation potentials at $E^1_{1/2}$ = 0 and $E^2_{1/2}$ = 0.14 V, respectively. The increased electron-withdrawing ability of acceptor **TQ** in chromophore **DTQD** has pulled the π-electrons from the electron-donating units, which results in the negatively shifted oxidation potential.

Since the reduction potential of some of the resulting chromophores is beyond the electrochemical window of the electrolyte, the LUMO levels are calculated from the equation $E_{LUMO} = E_g^{opt} + E_{HOMO}$.[17b] As shown in Table 1, the LUMO level of the resulting chromophores decreases from −2.46 V for chromophore **DQxD** to −3.37 V for chromophore **DTQD**, implying the different electron-withdrawing ability for the central pyrazine-based acceptors. A lower LUMO level suggests stronger electron-withdrawing ability and intramolecular charge transfer interactions, which results in lower band gap and bathochromically shifted absorption maximum (Figure 2). It can be concluded that a simple fusion of a benzene or thiophene ring on the electron-deficient pyrazine unit had significant effect on the modification of electron-withdrawing ability and tuning the LUMO level of the conjugated system.

Theoretical Approach. To have deep insight into the molecular geometries and electronic properties of the target chromophores, time-dependent density functional theory (TD-DFT) calculations were conducted with the Gaussian 03 program using the B3LYP method and 6-31G* basis set.[29] Figure 8 displays their optimized molecular structures together with the frontier molecular orbital profiles. It can be found that the dihedral angles between the central acceptor and the adjacent benzene ring are distinct and can be divided into three categories. As shown in Table 2, for chromophores **DQxD** and **DPzD**, the dihedral angles between the **Qx** or **Pz** and the neighboring benzene ring are calculated to be both 42°. However, chromophores **DBQD** and **DBPD** show a more twisted dihedral angle of 62 and 61°, respectively, which is obviously due to the increased steric hindrance between the fused benzene ring and the *ortho*-hydrogens on the adjacent phenylene group. This explains the 38 nm hypsochromic shift of the maximum absorption wavelength in the absorption spectrum of chromophore **DBQD** in comparison to that for chromophore **DPzD**. Moreover, for the thiophene-related two chromophores **DTPD** and **DTQD**, the dihedral angles between the thiophene ring in **TP** or **TQ** and the adjacent benzene ring decrease to 23 and 22°, respectively, due to the reduced steric hindrance between a benzene ring and a five-membered thiophene ring. Therefore, in addition to the stronger electron-donating ability of the thiophene ring in comparison to the benzene ring, chromophores **DTPD** and **DTQD** exhibit more planar molecular structures and more effective π-conjugation, which results in the more strengthened intramolecular interactions and lower band gap. These results are consistent with the experimentally observed absorption properties for the resulting chromophores (Figure 2).

As shown in Figure 8, all the chromophores demonstrate an overlap between HOMO and LUMO on the central acceptor unit, which facilitates the charge transfer from the two electron-donating arylamine centers to the electron-withdrawing pyrazine center.[30] Moreover, with the fusion of the benzene or thiophene ring on the central pyrazine unit, especially for chromophores **DBPD**, **DTPD**, and **DTQD**, the delocalization of HOMOs clearly extends to the fused benzene or thiophene ring in the acceptors. Therefore, a better overlap between the HOMO and the LUMO provides facile charge transfer from the electron donor to the acceptor.[30] To further compare the charge transfer processes in the resulting chromophores, the Mulliken and natural bond orbital (NBO) population analyses[31] are utilized to compare the partial charges on the donor and acceptor moieties. The calculated Mulliken and

Table 2. Calculated Dihedral Angles, Energy Levels, and Partial Charges from Mulliken and NBO Population Analyses

					Mulliken charge		NBO charge	
	dihedral angle (deg)[a]	E_g^{cal} (eV)	E_{HOMO} (eV)	E_{LUMO} (eV)	Q_D[b]	Q_A[c]	Q_D[b]	Q_A[c]
DQxD	42	3.35	−5.26	−1.91	0.0556	−0.1113	0.0214	−0.0428
DBQD	62	3.08	−5.32	−2.24	0.0557	−0.1113	0.0261	−0.0522
DPzD	42	2.80	−5.24	−2.44	0.0572	−0.1114	0.0319	−0.0638
DBPD	61	2.53	−5.25	−2.72	0.0578	−0.1155	0.0297	−0.0594
DTPD	23	2.69	−5.01	−2.32	0.1423	−0.2845	0.0352	−0.0704
DTQD	22	2.11	−4.90	−2.79	0.1434	−0.2868	0.0327	−0.0653

[a]Dihedral angle between the central acceptor and the adjacent benzene ring. [b]Partial charge on the electron donor. [c]Partial charge on the electron acceptor.

dx.doi.org/10.1021/jo500856k | J. Org. Chem. 2014, 79, 6480−6489

NBO charges for each subunit are listed in Table 2, which predicts the trend that, upon the fusion of either benzene or thiophene ring, both the Mulliken and NBO charges on the donor and acceptor moieties increase and the effect from the fusion of the thiophene ring is more significant than that of the benzene ring. This also explains the dramatically improved charge transfer interactions by extending the conjugation of pyrazine ring vertical to the bridge direction. Similar to the experimentally estimated HOMO levels for the chromophores, the calculated HOMO levels range from −5.26 to −4.9 eV (Table 2), although the electron-donating groups for all the chromophores are identical. This indicates that the inductive effect in the chromophores varies significantly from the electron-withdrawing ability of the acceptor groups. The calculated and experimental HOMO levels of the target chromophores are close to each other, while the calculated LUMO levels (Table 2) and maximum absorption wavelengths (Tables S2−S7) are different from the experimental ones. However, the qualitative trends of the theoretical LUMO levels and maximum absorption wavelengths are mostly similar to those experimentally determined ones.

CONCLUSIONS

In summary, a family of symmetrical D−A−D chromophores with pyrazine derivatives as acceptors has been designed and prepared successfully. It can be found that the six D−A−D chromophores exhibit different ICT interactions due to the various electron-withdrawing abilities of the central pyrazine derivatives. Fusing either a benzene or thiophene ring on the pyrazine acceptor unit can strengthen the ICT interactions and results in a bathochromically shifted ICT band. Upon the fusion of a benzene ring on the **Qx** moiety in chromophore **DQxD**, the ICT band is bathochromically shifted from 413 nm for **DQxD** to 493 nm for **DPzD**. However, when a single thiophene ring is fused on the **Qx** moiety instead of the benzene ring, an unusual bathochromic shift of 303 nm is observed for the ICT band of chromophore **DTQD**, which displays the maximum absorption wavelength at 716 nm. These results indicate that extending the conjugation of the pyrazine acceptor in an orthogonal direction to the D−A−D backbone can dramatically strengthen the ICT interactions and lower the band gap. Our findings will help us to understand the structure−property relationship of pyrazine-based semiconductors and control the charge transfer in pyrazine derivatives for the construction of low band gap materials.

EXPERIMENTAL SECTION

Materials and Reagents. All chemicals and reagents were purchased from commercial sources and used as received. THF and toluene were distilled from sodium benzophenone ketyl. DCM and chloroform were distilled from CaH_2. All reactions and manipulations were carried out under nitrogen with the use of standard inert atmosphere and Schlenk techniques. Dibromides 5,7-dibromothieno-[3,4-*b*]pyrazine and 5,8-dibromoquinoxaline were synthesized according to our previously reported procedures.[20]

Measurement and Characterizations. ^{1}H NMR (400 MHz) and ^{13}C NMR (100 MHz) spectra were recorded in $CDCl_3$, CD_2Cl_2, or THF-d_8 solutions. The chemical shifts were expressed in parts per million downfield from tetramethylsilane. The splitting patterns are designated as follows: s (singlet); d (doublet); t (triplet); m (multiplet). The UV−vis absorption spectra were measured on a dual beam scanning spectrophotometer using samples prepared as dilute solutions in 1 cm quartz cuvettes. Electrochemical redox potentials were obtained by CV and DPV measurements, which were performed using a typical three-electrode electrochemical cell in a solution of tetrabutylammonium hexafluorophosphate (0.1 M) in anhydrous DCM at a scan rate of 100 mV/s at room temperature under nitrogen. A glassy carbon electrode was used as the working electrode, a Pt wire as the counter electrode, and a Ag/Ag^+ electrode as the reference electrode. The potential of the reference electrode was calibrated with ferrocene. TD-DFT calculations were conducted with the Gaussian 03 program using the B3LYP method and 6-31G* basis set. The geometries were fully optimized in DCM solutions using the default convergence criteria without any constraints.

Synthesis of 1,4-Dibromophenazine (2). To a solution of $K_2Cr_2O_7$ (3.53 g, 12.00 mmol) in 2 M H_2SO_4 were added CH_2Cl_2 (200 mL) and catechol (0.66 g, 6.00 mmol). The mixture was stirred at room temperature for 15 min. Then the organic layer was separated with an aqueous layer, and the resulting 1,2-benzoquinone solution was used without further purification. To the organic layer were added 3,6-dibromobenzene-1,2-diamine (**1**) (266 mg, 1.00 mmol) and acetic acid (1 mL), and the mixture was heated at 70 °C for 8 h. After removal of the solvent, the residue was purified by flash column chromatography (silica gel, DCM/petroleum ether (PE) = 1/2). The slightly yellow solid 1,4-dibromophenazine was obtained with a yield of 47% (160 mg): ^{1}H NMR (400 MHz, $CDCl_3$, δ ppm) 8.41−8.38 (m, 2H), 8.04 (s, 2H), 7.95−7.92 (m, 2H); ^{13}C NMR (100 MHz, $CDCl_3$, δ ppm) 144.0, 141.1, 133.4, 132.1, 129.9, 124.3; HRMS (ESI, *m*/*z*) [(M + H)$^+$] calcd for $C_{12}H_7Br_2N_2$ 338.8956, found 338.8929.

Synthesis of 5,10-Dibromobenzo[*g*]quinoxaline (4). Under a nitrogen atmosphere, to a solution of 1,4-dibromonaphthalene-2,3-diamine (800 mg, 2.53 mmol) in ethanol (60 mL) was added 40 wt % glyoxal in water (1.0 mL), followed by 0.1 mL triethylamine. This mixture was stirred at 65 °C overnight. The formed dark green solid was filtered off and purified by flash column chromatography (silica gel, DCM/PE = 1/3): yield 89% (760 mg); ^{1}H NMR (400 MHz, $CDCl_3$, δ ppm) 9.03 (s, 2H), 8.70−8.68 (m, 2H), 7.77−7.74 (m, 2H); ^{13}C NMR (100 MHz, $CDCl_3$, δ ppm) 147.6, 146.6, 133.4, 129.3, 128.8, 125.3; HRMS (ESI, *m*/*z*) [(M + H)$^+$] calcd for $C_{12}H_7Br_2N_2$ 338.8956, found 338.8939.

Synthesis of 6,11-Dibromobenzo[*b*]phenazine (5). Compound 6,11-dibromobenzo[*b*]phenazine was synthesized similarly as described for synthesis of 1,4-dibromophenazine as a black solid in 41% yield (120 mg): ^{1}H NMR (400 MHz, CD_2Cl_2, δ ppm) 8.72−8.69 (m, 2H), 8.35−8.32 (m, 2H), 7.94−7.92 (m, 2H), 7.72−7.70 (m, 2H); ^{13}C NMR (100 MHz, CD_2Cl_2, δ ppm) 145.6, 145.1, 133.6, 132.4, 129.8, 128.9, 128.5, 124.8; HRMS (ESI, *m*/*z*) [(M + H)$^+$] calcd for $C_{16}H_9Br_2N_2$ 388.9112, found 388.9101.

General Procedure for Compounds DQxD, DBQD, DPzD, DBPD, and DTPD. Under a nitrogen atmosphere, dibromide (0.2 mmol), 4-diphenylaminophenylboronic acid (127 mg, 0.44 mmol), $Pd(PPh_3)_4$ (27 mg, 0.02 mmol), and K_2CO_3 (1.38 g, 0.01 mol) in a solution of H_2O (5 mL), toluene (7.5 mL), and THF (7.5 mL) were mixed together in a 100 mL Schlenk flask. The mixture was stirred and heated at 85 °C overnight. When the reaction was completed, the mixture was extracted with DCM two times. The combined organic solution was washed by brine and dried over anhydrous sodium sulfate. After removal of the solvent, the residue was purified by flash column chromatography (silica gel, DCM/PE = 1/2) to afford the desired product.

4,4′-(Quinoxaline-5,8-diyl)bis(*N*,*N*-diphenylaniline) (DQxD): 89% yield (190 mg), yellow solid; ^{1}H NMR (400 MHz, $CDCl_3$, δ ppm) 8.90 (s, 2H), 7.86 (s, 2H), 7.63 (d, 4H, *J* = 8.6 Hz), 7.30 (t, 8H, *J* = 7.8 Hz), 7.22−7.19 (m, 12H), 7.06 (t, 4H, *J* = 7.2 Hz); ^{13}C NMR (100 MHz, $CDCl_3$, δ ppm) 147.9, 147.6, 144.2, 141.5, 139.6, 132.2, 131.7, 130.2, 129.6, 125.1, 123.4, 122.8; MALDI-TOF *m*/*z* 616, calcd 616.3; HRMS (ESI, *m*/*z*) [(M + H)$^+$] calcd for $C_{44}H_{33}N_4$, 617.2705; found, 617.2703.

4,4′-(Benzo[*g*]quinoxaline-5,10-diyl)bis(*N*,*N*-diphenylaniline) (DBQD): 84% yield (150 mg), orange solid; ^{1}H NMR (400 MHz, THF-d_8, δ ppm) 8.78 (d, 2H, *J* = 1.2 Hz), 8.10−8.08 (m, 2H), 7.51−7.49 (m, 2H), 7.36−7.29 (m, 12H), 7.24−7.21 (m, 12H), 7.06−7.03 (m, 4H); ^{13}C NMR (100 MHz, THF-d_8, δ ppm) 148.1, 147.3, 145.8, 138.6, 137.6, 132.8, 132.6, 131.3, 129.4, 127.4, 126.3, 124.8,

dx.doi.org/10.1021/jo500856k | J. Org. Chem. 2014, 79, 6480−6489

123.1, 122.3; MALDI-TOF *m/z* 666, calcd 666.3; HRMS (ESI, *m/z*) [(M + H)$^+$] calcd for $C_{48}H_{35}N_4$ 667.2862, found 667.2850.

4,4′-(Phenazine-1,4-diyl)bis(*N*,*N*-diphenylaniline) (DPzD): 87% yield (120 mg), red solid; ^{1}H NMR (400 MHz, CD_2Cl_2, δ ppm) 8.13−8.10 (m, 2H), 7.81 (s, 2H), 7.75−7.72 (m, 2H), 7.68 (d, 4H, *J* = 8.5 Hz), 7.23 (t, 8H, *J* = 7.8 Hz), 7.14−7.11 (m, 12H), 6.99 (t, 4H, *J* = 7.3 Hz); ^{13}C NMR (100 MHz, CD_2Cl_2, δ ppm) 147.9, 147.7, 142.6, 142.1, 139.3, 132.6, 131.9, 130.6, 130.0, 129.6, 125.0, 123.4, 122.7; MALDI-TOF *m/z* 666, calcd 666.3; MALDI-TOF *m/z* 666, calcd 666.3; HRMS (ESI, *m/z*) [(M + H)$^+$] calcd for $C_{48}H_{35}N_4$ 667.2862, found 667.2844.

4,4′-(Benzo[*b*]phenazine-6,11-diyl)bis(*N*,*N*-diphenylaniline) (DBPD): 81% yield (60 mg), black solid; ^{1}H NMR (400 MHz, CD_2Cl_2, δ ppm) 8.03−8.00 (m, 4H), 7.68−7.66 (m, 2H), 7.40−7.36 (m, 6H), 7.30−7.26 (m, 8H), 7.22−7.20 (m, 12H), 7.02 (t, 4H, *J* = 7.1 Hz); ^{13}C NMR (100 MHz, CD_2Cl_2, δ ppm) 148.0, 147.5, 143.8, 138.6, 138.0, 133.4, 132.9, 131.4, 130.7, 130.3, 129.6, 127.6, 126.4, 125.0, 123.4, 122.5; MALDI-TOF *m/z* 716, calcd 716.3; HRMS (ESI, *m/z*) [(M + H)$^+$] calcd for $C_{52}H_{37}N_4$ 717.3018, found 717.2996.

4,4′-(Thieno[3,4-*b*]pyrazine-5,7-diyl)bis(*N*,*N*-diphenylaniline) (DTPD): 87% yield (185 mg), black solid; ^{1}H NMR (400 MHz, $CDCl_3$, δ ppm) 8.46 (s, 2H), 8.00−7.98 (m, 4H), 7.30−7.26 (m, 8H), 7.18−7.14 (m, 12H), 7.08−7.04 (m, 4H); ^{13}C NMR (100 MHz, $CDCl_3$, δ ppm) 147.8, 147.5, 144.0, 139.8, 131.5, 129.6, 129.0, 127.1, 125.0, 123.6, 123.5; MALDI-TOF *m/z* 622, calcd 622.2; HRMS (ESI, *m/z*) [(M + H)$^+$] calcd for $C_{42}H_{31}N_4S$ 623.2269, found 623.2255.

Synthesis of 4,4′-(Thieno[3,4-*b*]quinoxaline-1,3-diyl)bis(*N*,*N*-diphenylaniline) (DTQD). Compound 2,5-bis(4-(diphenylamino)-phenyl)thiophene-3,4-diamine was synthesized according to previously reported literature.[32] Compound **DTPD** was synthesized similarly as described for synthesis of 1,4-dibromophenazine, black solid, 35% yield (50 mg): ^{1}H NMR (400 MHz, CD_2Cl_2, δ ppm) 8.21−8.19 (m, 4H), 7.82−7.80 (m, 2H), 7.50−7.48 (m, 2H), 7.23 (t, 8H, *J* = 7.6 Hz), 7.10−7.09 (m, 12H), 7.00 (t, 4H, *J* = 7.2 Hz); ^{13}C NMR (100 MHz, CD_2Cl_2, δ ppm) 147.5, 143.9, 130.7, 130.6, 129.6, 128.6, 125.0, 123.6, 123.4; MALDI-TOF *m/z* 672, calcd 672.2; HRMS (ESI, *m/z*) [(M + H)$^+$] calcd for $C_{46}H_{33}N_4S$ 673.2426, found 673.2422.

■ ASSOCIATED CONTENT

Ⓢ Supporting Information

^{1}H and ^{13}C NMR and MALDI-TOF MS spectra, computational details, and X-ray crystallographic data (CIF files) for the related compounds. This material is available free of charge via the Internet at http://pubs.acs.org.

■ AUTHOR INFORMATION

Corresponding Author

*E-mail: zhougang@fudan.edu.cn. Tel: +86-21-5163-0350. Fax: +86-21-5163-0345.

Notes

The authors declare no competing financial interest.

■ ACKNOWLEDGMENTS

This work was financially supported by the National Basic Research Program of China (2011CB933302), the National Natural Science Foundation of China (51273045, 21201037), NCET-12-0122, STCSM (12JC1401500), Shanghai Leading Academic Discipline Project (B108), and Jiangsu Major Program (BY2010147).

■ REFERENCES

(1) (a) Tang, C. W.; Vanslyke, S. A. *Appl. Phys. Lett.* **1987**, *51*, 913. (b) Müller, C. D.; Falcou, A.; Reckefuss, N.; Rojahn, M.; Wiederhirn, V.; Rudati, P.; Frohne, H.; Nuyken, O.; Becker, H.; Meerholz, K. *Nature* **2003**, *421*, 829.

(2) (a) Tang, C. W. *Appl. Phys. Lett.* **1986**, *48*, 183. (b) Wohrle, D.; Meissner, D. *Adv. Mater.* **1991**, *3*, 129.

(3) (a) Tsumura, A.; Koezuka, H.; Ando, K. *Appl. Phys. Lett.* **1986**, *49*, 1210. (b) Bao, Z.; Lovinger, A. J.; Brown, J. *J. Am. Chem. Soc.* **1998**, *120*, 207. (c) Zhou, Y.; Liu, W.-J.; Ma, Y.; Wang, H.; Qi, L.; Cao, Y.; Wang, J.; Pei, J. *J. Am. Chem. Soc.* **2007**, *129*, 12386.

(4) Williams, D. J. *Angew. Chem., Int. Ed. Engl.* **1984**, *23*, 690.

(5) (a) Martínez-Máñez, R.; Sancenón, F. *Chem. Rev.* **2003**, *103*, 4419. (b) Thomas, S. W., III; Joly, G. D.; Swager, T. M. *Chem. Rev.* **2007**, *107*, 1339.

(6) Ajayaghosh, A. *Chem. Soc. Rev.* **2003**, *32*, 181.

(7) (a) Ying, W.; Yang, J.; Wielopolski, M.; Moehl, T.; Moser, J.-E.; Comte, P.; Hua, J.; Zakeeruddin, S. M.; Tian, H.; Grätzel, M. *Chem. Sci.* **2014**, *5*, 206. (b) Bunz, U. H. F. *Chem.—Eur. J.* **2009**, *15*, 6780. (c) Gao, B.; Wang, M.; Cheng, Y.; Wang, L.; Jing, X.; Wang, F. *J. Am. Chem. Soc.* **2008**, *130*, 8297. (d) Miao, S.; Smith, M. D.; Bunz, U. H. F. *Org. Lett.* **2006**, *8*, 757. (e) Bunz, U. H. F.; Engelhart, J. U.; Lindner, B. D.; Manuel Schaffroth, M. *Angew. Chem., Int. Ed.* **2013**, *52*, 3810. (f) Schaffroth, M.; Lindner, B. D.; Vasilenko, V.; Rominger, F.; Bunz, U. H. F. *J. Org. Chem.* **2013**, *78*, 3142. (g) Engelhart, J. U.; Lindner, B. D.; Tverskoy, O.; Schaffroth, M.; Rominger, F.; Bunz, U. H. F. *J. Org. Chem.* **2013**, *78*, 1249. (h) An, C.; Puniredd, S. R.; Guo, X.; Stelzig, T.; Zhao, Y.; Pisula, W.; Baumgarten, M. *Macromolecules* **2014**, *47*, 979. (i) Achelle, S.; Baudequin, C.; Plé, N. *Dyes Pigm.* **2013**, *98*, 575.

(8) (a) Wang, E.; Hou, L.; Wang, Z.; Ma, Z.; Hellström, S.; Zhuang, W.; Zhang, F.; Inganäs, O.; Andersson, M. R. *Macromolecules* **2011**, *44*, 2067. (b) Zhang, Y.; Zou, J.; Yip, H.-L.; Chen, K.-S.; Zeigler, D. F.; Sun, Y.; Jen, A. K.-Y. *Chem. Mater.* **2011**, *23*, 2289.

(9) Campos, L. M.; Tontcheva, A.; Günes, S.; Sonmez, G.; Neugebauer, H.; Sariciftci, N. S.; Wudl, F. *Chem. Mater.* **2005**, *17*, 4031.

(10) Blouin, N.; Michaud, A.; Gendron, D.; Wakim, S.; Blair, E.; Neagu-Plesu, R.; Belletête, M.; Durocher, G.; Tao, Y.; Leclerc, M. *J. Am. Chem. Soc.* **2008**, *130*, 732.

(11) Chen, H.-C.; Chen, Y.-H.; Liu, C.-C.; Chien, Y.-C.; Chou, S.-W.; Chou, P.-T. *Chem. Mater.* **2012**, *24*, 4766.

(12) (a) Zhang, F.; Bijleveld, J.; Perzon, E.; Tvingstedt, K.; Barrau, S.; Inganäsab, O.; Andersson, M. R. *J. Mater. Chem.* **2008**, *18*, 5468. (b) Zoombelt, A. P.; Fonrodona, M.; Turbiez, M. G. R.; Wienkab, M. M.; Janssen, R. A. J. *J. Mater. Chem.* **2009**, *19*, 5336. (c) Schulz, G. L.; Mastalerz, M.; Ma, C.-Q.; Wienk, M.; Janssen, R.; Bäuerle, P. *Macromolecules* **2013**, *46*, 2141.

(13) Zoombelt, A. P.; Fonrodona, M.; Wienk, M. M.; Sieval, A. B.; Hummelen, J. C.; Janssen, R. A. J. *Org. Lett.* **2009**, *11*, 903.

(14) Zhang, Y.; Zou, J.; Yip, H.-L.; Chen, K.-S.; Davies, J. A.; Sun, Y.; Jen, A. K.-Y. *Macromolecules* **2011**, *44*, 4752.

(15) Du, X.; Qi, J.; Zhang, Z.; Ma, D.; Wang, Z. Y. *Chem. Mater.* **2012**, *24*, 2178.

(16) (a) Li, H.; Kim, F. S.; Ren, G.; Hollenbeck, E. C.; Subramaniyan, S.; Jenekhe, S. A. *Angew. Chem., Int. Ed.* **2013**, *52*, 5513. (b) Ye, Q.; Chang, J.; Huang, K.-W.; Shi, X.; Wu, J.; Chi, C. *Org. Lett.* **2013**, *15*, 1194.

(17) (a) Qian, G.; Dai, B.; Luo, M.; Yu, D.; Zhan, J.; Zhang, Z.; Ma, D.; Wang, Z. Y. *Chem. Mater.* **2008**, *20*, 6208. (b) Tao, T.; Ma, B.-B.; Peng, Y.-X.; Wang, X.-X.; Huang, W.; You, X.-Z. *J. Org. Chem.* **2013**, *78*, 8669.

(18) (a) Teng, C.; Yang, X.; Yang, C.; Tian, H.; Li, S.; Wang, X.; Hagfeldt, A.; Sun, L. *J. Phys. Chem. C* **2010**, *114*, 11305. (b) Mao, J.; He, N.; Ning, Z.; Zhang, Q.; Guo, F.; Chen, L.; Wu, W.; Hua, J.; Tian, H. *Angew. Chem., Int. Ed.* **2012**, *51*, 9873.

(19) Miyaura, N.; Suzuki, A. *Chem. Rev.* **1995**, *95*, 2457.

(20) (a) Lu, X.; Zhou, G.; Wang, H.; Feng, Q.; Wang, Z.-S. *Phys. Chem. Chem. Phys.* **2012**, *14*, 4802. (b) Lu, X.; Feng, Q.; Lan, T.; Zhou, G.; Wang, Z.-S. *Chem. Mater.* **2012**, *24*, 3179.

(21) Tsubata, Y.; Suzuki, T.; Miyashi, T. *J. Org. Chem.* **1992**, *57*, 6749.

(22) Wei, P.; Duan, L.; Zhang, D.; Qiao, J.; Wang, L.; Wang, R.; Dong, G.; Qiu, Y. *J. Mater. Chem.* **2008**, *18*, 806.

(23) (a) Kenning, D. D.; Mitchell, K. A.; Calhoun, T. R.; Funfar, M. R.; Sattler, D. J.; Rasmussen, S. C. *J. Org. Chem.* **2002**, *67*, 9073. (b) Bijleveld, J. C.; Shahid, M.; Gilot, J.; Wienk, M. M.; Janssen, R. A. J. *Adv. Funct. Mater.* **2009**, *19*, 3262.
(24) Miao, S.; Brombosz, S. M.; Schleyer, P. R.; Wu, J. I.; Barlow, S.; Marder, S. R.; Hardcastle, K. I.; Bunz, U. H. F. *J. Am. Chem. Soc.* **2008**, *130*, 7339.
(25) Chou, H.-H.; Chen, Y.-C.; Huang, H.-J.; Lee, T.-H.; Lin, J. T.; Tsai, C.; Chen, K. *J. Mater. Chem.* **2012**, *22*, 10929.
(26) Clarke, T. M.; Gordon, K. C.; Kwok, W. M.; Phillips, D. L.; Officer, D. L. *J. Phys. Chem. A* **2006**, *110*, 7696.
(27) (a) Heckmann, A.; Lambert, C. *Angew. Chem., Int. Ed.* **2012**, *51*, 326. (b) Hankache, J.; Wenger, O. S. *Chem. Rev.* **2011**, *111*, 5138.
(28) (a) McCulloch, I.; Ashraf, R. S.; Biniek, L.; Bronstein, H.; Combe, C.; Donaghey, J. E.; James, D. I.; Nielsen, C. B.; Schroeder, B. C.; Zhang, W. *Acc. Chem. Res.* **2012**, *45*, 714. (b) Neuvonen, H.; Neuvonen, K.; Fülöp, F. *J. Org. Chem.* **2006**, *71*, 3141. (c) Fersner, A.; Karty, J. M.; Mo, Y. *J. Org. Chem.* **2009**, *74*, 7245.
(29) Frisch, M. J.; Trucks, G. W.; Schlegel, H. B.; Scuseria, G. E.; Robb, M. A.; Cheeseman, J. R.; Montgomery, J. A., Jr.; Vreven, J. T.; Kudin, K. N.; Burant, J. C.; Millam, J. M.; Iyengar, S. S.; Tomasi, J.; Barone, V.; Mennucci, B.; Cossi, M.; Scalmani, G.; Rega, N.; Petersson, G. A.; Nakatsuji, H.; Hada, M.; Ehara, M.; Toyota, K.; Fukuda, R.; Hasegawa, J.; Ishida, M.; Nakajima, T.; Honda, Y.; Kitao, O.; Nakai, H.; Klene, M.; Li, X.; Knox, J. E.; Hratchian, H. P.; Cross, J. B.; Bakken, V.; Adamo, C.; Jaramillo, J.; Gomperts, R.; Stratmann, R. E.; Yazyev, O.; Austin, A. J.; Cammi, R.; Pomelli, C.; Ochterski, J. W.; Ayala, P. Y.; Morokuma, K.; Voth, G. A.; Salvador, P.; Dannenberg, J. J.; Zakrzewski, V. G.; Dapprich, S.; Daniels, A. D.; Strain, M. C.; Farkas, O.; Malick, D. K.; Rabuck, A. D.; Raghavachari, K.; Foresman, J. B.; Ortiz, J. V.; Cui, Q.; Baboul, A. G.; Clifford, S.; Cioslowski, J.; Stefanov, B. B.; Liu, G.; Liashenko, A.; Piskorz, P.; Komaromi, I.; Martin, R. L.; Fox, D. J.; Keith, T.; Al-Laham, M. A.; Peng, C. Y.; Nanayakkara, A.; Challacombe, M.; Gill, P. M. W.; Johnson, B.; Chen, W.; Wong, M. W.; Gonzalez, C.; Pople, J. A. *Gaussian03*, revision C.02; Gaussian Inc.: Wallingford, CT, 2004.
(30) Luo, J.; Xu, M.; Li, R.; Huang, K.-W.; Jiang, C.; Qi, Q.; Zeng, W.; Zhang, J.; Chi, C.; Wang, P.; Wu, J. *J. Am. Chem. Soc.* **2014**, *136*, 265.
(31) Reed, A. E.; Curtiss, L. A.; Weinhold, F. *Chem. Rev.* **1988**, *88*, 899.
(32) Gao, B.; Xia, D.; Geng, Y.; Cheng, Y.; Wang, L. *Tetrahedron Lett.* **2010**, *51*, 1919.